

Article

Mn-Ce-V-WO_x/TiO₂ SCR Catalysts: Catalytic Activity, Stability and Interaction among Catalytic Oxides

Xuteng Zhao ¹, Lei Mao ¹ and Guojun Dong ^{1,2,*}

¹ School of Material Science and Chemical Engineering, Harbin Engineering University, Harbin 150001, China; zhaoxuteng@hrbeu.edu.cn (X.Z.); maolei0119@163.com (L.M.)

² Key Laboratory of Superlight Material and Surface Technology of Ministry of Education, College of Material Science and Chemical Engineering, Harbin Engineering University, Harbin 150001, China

* Correspondence: dgj1129@163.com; Tel.: +86-180-4508-1027

Received: 28 January 2018; Accepted: 6 February 2018; Published: 12 February 2018

Abstract: A series of Mn-Ce-V-WO_x/TiO₂ composite oxide catalysts with different molar ratios (active components/TiO₂ = 0.1, 0.2, 0.3, 0.6) have been prepared by wet impregnation method and tested in selective catalytic reduction (SCR) of NO by NH₃ in a wide temperature range. These catalysts were also characterized by X-ray diffraction (XRD), Transmission Electron Microscope (TEM), in situ Fourier Transform infrared spectroscopy (in situ FTIR), H₂-Temperature programmed reduction (H₂-TPR) and X-ray photoelectron spectroscopy (XPS). The results show the catalyst with a molar ratio of active components/TiO₂ = 0.2 exhibits highest NO conversion value between 150 °C to 400 °C and good resistance to H₂O and SO₂ at 250 °C with a gas hourly space velocity (GHSV) value of 40,000 h⁻¹. Different oxides are well dispersed and interact with each other. NH₃ and NO are strongly adsorbed on the catalyst surface and the adsorption of the reactant gas leads to a redox cycle with the valence state change among the surface oxides. The adsorption of SO₂ on Mn⁴⁺ and Ce⁴⁺ results in good H₂O and SO₂ resistance of the catalyst, but the effect of Mn and Ce are more than superior water and sulfur resistance. The diversity of valence states of the four active components and their high oxidation-reduction performance are the main reasons for the high NO conversion in this system.

Keywords: composite oxide catalyst; NH₃-SCR of NO; lifetime; H₂O and SO₂ resistance

1. Introduction

The selective catalytic reduction (SCR) of NO_x with NH₃ in the presence of O₂ has been widely used to control the emissions of NO_x from mobile and stationary sources, such as coal-fired power plants and automobiles [1–4]. V₂O₅-WO₃/TiO₂ is the most used commercial catalyst for SCR of NO_x at a relatively high temperature platform of 300 °C to 400 °C [5–7]. However, the drawbacks of this catalyst system cannot be ignored. The operating temperature window is narrow and it has low catalytic activity for deNO_x at low temperature, for instance. Moreover, the catalytic performance can be seriously deactivated by H₂O and SO₂ in the emission [8–10]. Therefore, a low temperature catalyst with good resistance to SO₂ and H₂O is urgently needed for the SCR system to improve the situation.

So far, a lot of research has been done. Manganese-containing catalysts have attracted much attention due to their relatively high catalytic activity for the conversion of NO_x at low temperature, including Ni-MnO_x/TiO₂ [6], MnO_x-TiO₂ [11,12], Cr-MnO_x [13], Ce-MnO_x [14,15] and Ca-MnO_x/TiO₂ [10]. Fang et al. [16] have compared the conversion of NO on MnO_x/TiO₂, MnO_x/CNT and nano-flaky MnO_x/CNT and found that nano-flaky MnO_x/CNTs presents favourable stability, H₂O resistance and better NO-SCR activity at a more extensive operating temperature window between 150 °C to 300 °C. However, SO₂ leads to the irreversible deactivation of MnO_x/TiO₂ [9]. In recent years,

it has been reported that Ce-based catalysts reveal excellent SCR activity in the presence of SO₂ at 300–400 °C [17–19]. Yang and co-workers [18] have investigated the effect of SO₂ on the SCR reaction over CeO₂. The results have indicated that the adsorption of NH₃ over CeO₂ is obviously promoted with the sulfation of CeO₂, resulting in an obvious promotion of the Eley–Rideal mechanism.

In many cases, one or two active components can hardly handle all the situations of the SCR system. In this work, four elements of manganese, cerium, vanadium and tungsten have been used as the active components, with a reduction in the amount of vanadium. Then, a series of Mn-Ce-V-WO_x/TiO₂ composite oxide catalysts with different molar ratios of active components/TiO₂ have been prepared by an impregnation method. In addition, X-ray diffraction (XRD), Transmission electron microscopy (TEM), in situ Fourier transform infrared (FT-IR) spectroscopy, H₂ temperature-programmed reduction (H₂-TPR) and X-ray photoelectron spectroscopy (XPS) have been measured. The catalyst with a molar ratio of 0.2 exhibits the highest conversion of NO between 150 °C to 400 °C at a gas hourly space velocity (GHSV) of 40,000 h⁻¹. This catalyst shows long lifetime and superior resistance to H₂O and SO₂ at 250 °C. It is remarkable to note that the catalyst is not deactivated at all. Moreover, the analysis results also prove that the oxides on the catalyst surface interact with each other and enhance the redox properties of the oxides and the adsorption of reaction gas, resulting in a redox cycle with the valence state change of the surface oxides. This is probably the main reason for its unique performance.

2. Results and Discussion

2.1. Catalytic Behavior

All SCR activity of catalysts have been tested several times and error analysis have been performed, shown in the form of error bars in the figures. Figure 1A shows the SCR performances of Mn-Ce-V-WO_x/TiO₂ composite oxide catalysts with different molar ratios of active components/TiO₂ = 0.1, 0.2, 0.3, 0.6. For comparison, the SCR performances of V₂O₅/TiO₂, WO₃/TiO₂, MnO₂/TiO₂, CeO₂/TiO₂ and TiO₂ are given in Figure 1B. Compared with the single-component catalysts, composite catalysts show better catalytic activity. The NO conversion of all single component catalysts is less than 40% before 250 °C, while all Mn-Ce-V-WO_x/TiO₂ composite catalysts are more than 70% from 150 °C to 350 °C. Among them, the NO conversion of the catalyst with active components/TiO₂ = 0.2 molar ratio is even above 90% from 150 °C to 400 °C. Obviously, the addition of various active components can significantly improve the catalytic activity. The similar condition has also been observed through evaluating the SCR performances of two/three-components catalysts (Figure S1 in the Supplementary Materials). The catalytic activity of the three-components of MnO₂-V₂O₅-WO₃/TiO₂ and CeO₂-V₂O₅-WO₃/TiO₂ is significantly higher than that of reference catalysts. Furthermore, remarkably, the performance of CeO₂-V₂O₅-WO₃/TiO₂ is better than MnO₂-V₂O₅-WO₃/TiO₂, especially between 200 to 300 °C. It can be inferred that the effect of MnO₂ and CeO₂ on the V₂O₅-WO₃/TiO₂ catalyst is different. Moreover, with temperature increasing, the SCR activity of the Mn-Ce-V-WO_x/TiO₂ catalyst with the highest amount of loading decreases obviously, but others remain (shown in Figure 1A). It should also be mentioned that the catalyst with molar ratio of active components/TiO₂ = 0.2 has the highest catalytic performance at 150 °C. Thus, the optimal molar ratio (Mn-Ce-V-WO_x/TiO₂ = 0.2) is obtained, and the catalytic performance will drop when the ratio is low or high, especially when it is high. These results may be due to the different dispersion of the active components on the support surface and the strong interaction among them. Further explanation will be elaborated in the following analyses.

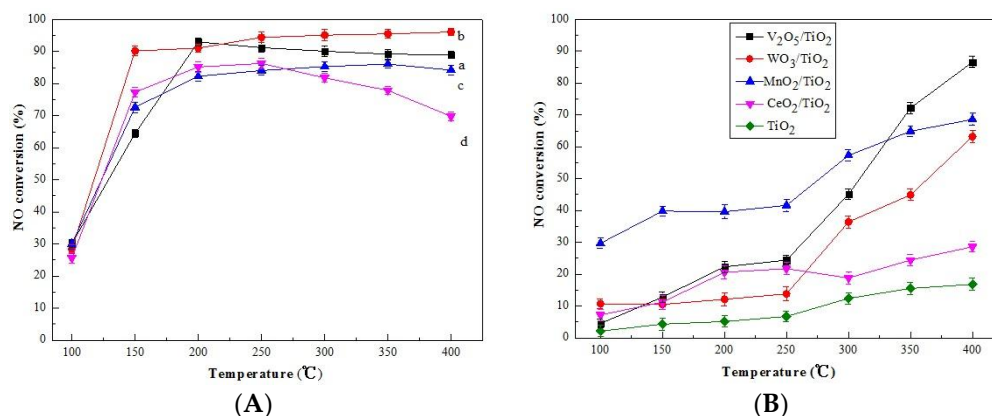


Figure 1. (A) Selective catalytic reduction (SCR) activity of Mn-Ce-V-WO_x/TiO₂ composite catalysts with the molar ratio of active components/TiO₂ at different values: (a) 0.1; (b) 0.2; (c) 0.3; (d) 0.6. (B) SCR activity of V₂O₅/TiO₂, WO₃/TiO₂, MnO₂/TiO₂, CeO₂/TiO₂ and TiO₂. Reaction conditions: [NO] = [NH₃] = 1500 ppm, [O₂] = 3%, gas hourly space velocity (GHSV) = 40,000 h⁻¹.

2.2. XRD Analysis

The XRD patterns of the Mn-Ce-V-WO_x/TiO₂ catalysts are shown in Figure 2. The XRD diffractions of the catalyst with the molar ratio of Mn-Ce-V-WO_x/TiO₂ = 0.1 are well indexed to anatase TiO₂ (JCPDS 21-1272) [20,21], indicating that active components are well dispersed on the surface of support. When the molar ratio reaches 0.2, the active components on the surface of the support begins to aggregate, but no strong diffraction peaks of crystal phase appear. If the molar ratio continues to be increased to 0.6, crystalline phases of all active components appear and TiO₂ peaks are diluted. The results are consistent with the SCR performances. Catalytic activity could be improved with the transition of active components from highly dispersed state to slightly aggregated state, yet a large amount of components' aggregation will also decrease the catalytic activity [22].

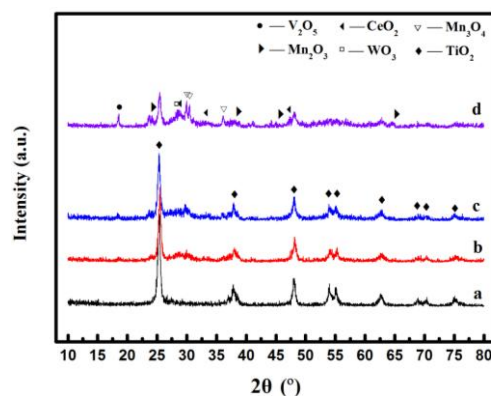


Figure 2. X-ray diffraction (XRD) patterns of Mn-Ce-V-WO_x/TiO₂ composite oxide catalysts with different molar ratio of active components/TiO₂: (a) 0.1; (b) 0.2; (c) 0.3; (d) 0.6.

XRD patterns of the reference catalysts are shown in Figure S2 in the Supplementary Materials. It can be seen that the reference catalysts with a single component only have the diffraction peak of anatase TiO₂. Interestingly, weak diffraction peaks of V₂O₅ and WO₃ are observed at approximately 23.2° and 34.3° in the spectrum of V₂O₅-WO₃/TiO₂ catalyst and 17.9°, 29.1°, 29.3° and 36.1° in the spectrum of MnO₂-V₂O₅-WO₃/TiO₂ catalyst, but the peaks of these angles disappear in the cerium containing systems; even the peaks of CeO₂ and MnO₂ have not appeared with the same molar ratio components added. The addition of Ce can be well dispersed, meanwhile, it can make other active components disperse more uniformly and avoid the large aggregation of active components on the

support surface, which can make it easier for all active components to contact the reaction gas and improve the catalytic activity of this catalyst system.

2.3. TEM and HRTEM Analysis

TEM images of the catalyst with a molar ratio of 0.2 are presented in Figure 3. The diameter of the catalyst particle is about 20 nm (Figure 3a,b). It is similar to TiO₂ support. The HRTEM micrographs (Figure 3c,d) display better defined contours, exhibiting higher crystalline order (Figure 3e–h). The d-spacing is measured at ca. 0.352 nm, ascribable to the (101) crystal planes of anatase TiO₂. The detected spacing from different positions is the same, matching well with the XRD pattern. The result further indicates that active components are well dispersed on the surface. The addition of four active components occupy more positions on the surface of support, resulting in an increase of acidic sites exposed on the surface, which improves the ability of NH₃ adsorption; this indirectly corresponds to the in situ FTIR test results of NH₃ adsorption characteristic peak occurring at high temperature in the following.

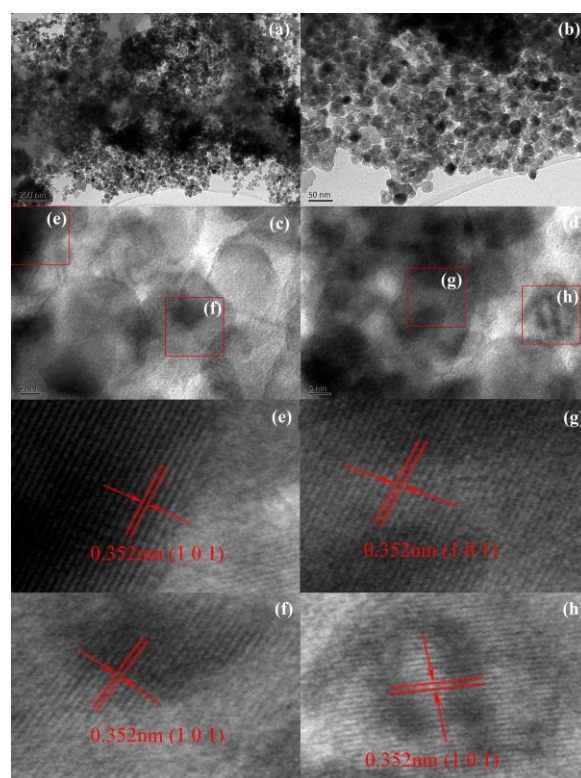


Figure 3. Transmission Electron Microscopy (TEM) and High Resolution Transmission Electron Microscopy (HRTEM) images of Mn-Ce-V-WO_x/TiO₂ catalyst with molar ratio of 0.2: (a,b) TEM images; (c,d) HRTEM images; (e,f) amplified images of (c); (g,h) amplified images of (d).

High Resolution Transmission Electron Microscopy (HRTEM) images of the reference catalysts with a molar ratio of 0.6 are presented in Figure S3 in the Supplementary Materials. Compared with the former, HRTEM images of the 0.6-ratio catalyst show different diffraction fringes with different distances. Only the spacing of the representative lattice fringes and the corresponding crystal planes are shown and corresponding crystals of active components are detected, indicating that mass aggregation of active components have appeared on the support surface. The results are similar to XRD analysis, and specific information is presented in Supplementary Materials. However, there is no characteristic fringes of TiO₂, indicating that TiO₂ may be completely covered by the active components.

2.4. Catalyst Stability and H₂O/SO₂ Resistance

The catalyst with the best SCR performance has been selected for the stability and H₂O/SO₂ resistance tests. From the above information of activity tests, catalysts begin to remain stable at 250 °C, and the reaction may reach balance at this temperature. So, H₂O/SO₂ resistance and the 100 h stability test of the catalyst have been performed at 250 °C, as Figure 4 and Figure S4 in the Supplementary Materials present, respectively. It can be seen that the activity of the catalyst remains at about 95.3% during 100 h with small fluctuations, and no decline is observed, which indicates that the catalyst has a longer service life. Furthermore, it is obvious that the SCR activity maintains a very high NO conversion with small fluctuations when 5 vol % H₂O, 100 ppm SO₂ or both are introduced into the typical reactant gas. The same results have been obtained after repeating the test several times. It has been reported that MnO₂, V₂O₅ and WO₃ are easily irreversibly deactivated by SO₂; only CeO₂ shows high activity in the presence of SO₂ [6,7,9]. In this research, although MnO₂ may still be attacked by SO₂, the adulteration of CeO₂ is significant to the catalyst for resisting the effect of SO₂. The addition of these two elements makes V and W less affected by SO₂ in the system. The result also indicates that the Mn-Ce-V-WO_x/TiO₂ catalyst with molar ratio of active components/TiO₂ = 0.2 has strong resistance to H₂O and SO₂. However, it cannot be assumed that the addition of Mn and Ce is simply attacked instead of V and W because the high NO conversion of the catalyst can still last a long time rather than being deactivated quickly in the presence of SO₂ and H₂O. There is a stronger interaction among the four active ingredients and the role of each element is crucial. Further investigations on the adsorption of reactive molecules and the effects of SO₂ and H₂O on the catalyst have been performed by in situ FTIR below.

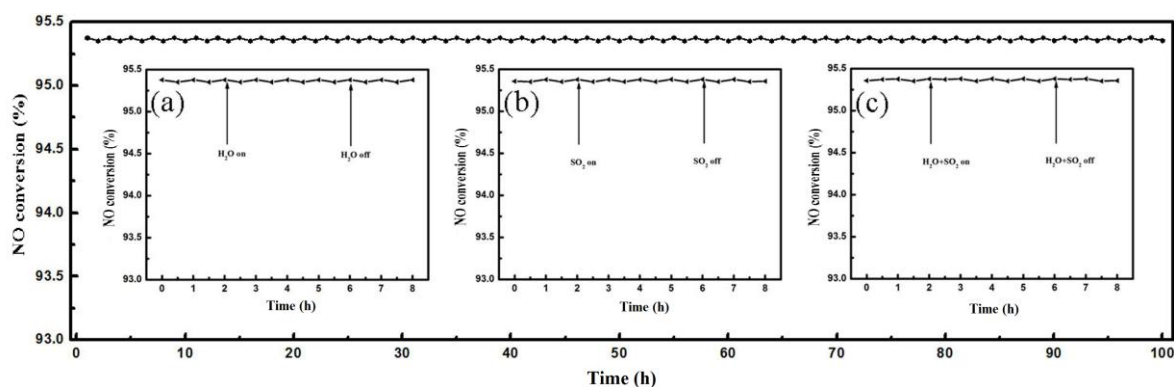


Figure 4. H₂O and SO₂ resistance of Mn-Ce-V-WO_x/TiO₂ catalyst with molar ratio of 0.2 at 250 °C: insert (a–c) H₂O and SO₂ resistance. Reaction conditions: [NO] = [NH₃] = 1500 ppm, [O₂] = 3%, [H₂O] = 5%, [SO₂] = 100 ppm, GHSV = 40,000 h⁻¹.

2.5. In Situ FTIR Analysis

The adsorption, transformation and desorption of the reactant gas on the catalyst's surface play an important role in the SCR reaction and they influence the reaction process. Under the condition of continuous exposure of typical reactant gas with or without SO₂, the in situ FTIR spectra of the catalyst with a molar ratio of 0.2 are shown in Figure 5. Several bands at 975, 1208, 1437, 1596, 1670, 3164, 3260, 3353 and 3395 cm⁻¹ are observed under the condition of continuous exposure of typical reactant gas without SO₂ (shown in Figure 5a). The bands at 975 and 1670 cm⁻¹ disappear over 150 °C, pointing to NH₄⁺ species on Brønsted acid sites [23,24]. Then, ν(N–H) and δ(N–H) bands of NH₃ adsorbed on Lewis sites at 1208 cm⁻¹ and between 3100 and 3400 cm⁻¹ are observed [25,26]. Additionally, the band at 1437 cm⁻¹ weakens gradually with increasing temperature, but exists even at 400 °C. So, it should be assigned to the adsorption of the nitro specie on the catalyst surface [27]. Moreover, the band at 1596 cm⁻¹ is attributed to the characteristic band of bridged nitrate species and it is not detected when the temperature is higher than 150 °C due to its poor stability. It can be concluded that NH₃

and NO are strongly adsorbed on the catalyst surface even when the temperature reaches 400 °C, and the adsorption of NH₃ on Lewis acid sites and NO have strong interaction with catalyst surface oxides. The strong interaction on the support surface promotes the strong adsorption of NH₃ and the formation of nitrate species. At 400 °C, the activity of the catalyst remains at 90%, indicating that the catalyst still has a SCR reaction at this temperature. The results correspond well to the previous SCR activity test.

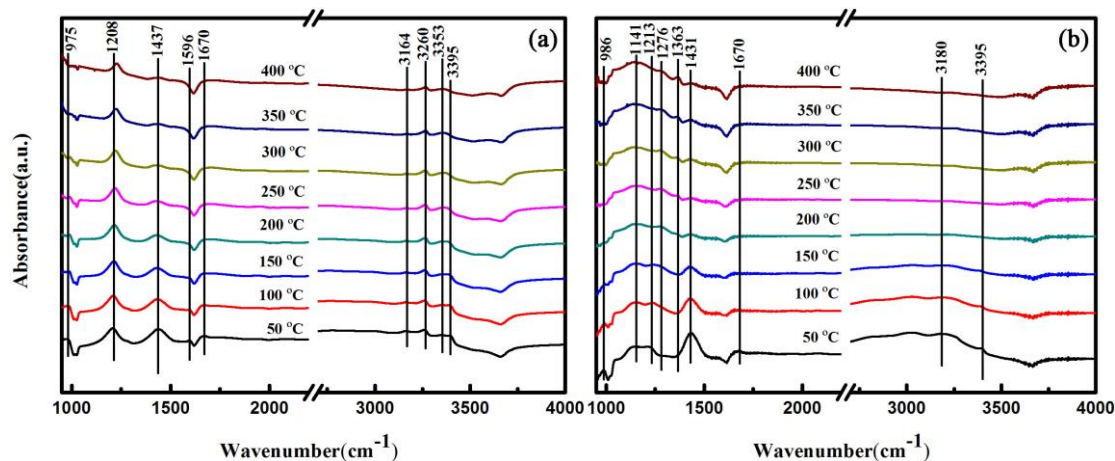


Figure 5. In situ Fourier Transform infrared spectroscopy (in situ FTIR) spectra of the catalyst with molar ratio of 0.2 under the condition of continuous exposure of typical reactant gas with or without SO₂: (a) without SO₂; (b) with SO₂.

When SO₂ is introduced into the typical reactant gas, several new bands at 986, 1141, 1213, 1276 and 1363 cm⁻¹ have appeared (Figure 5b). The band at 1141 cm⁻¹ is attributed to the stretching motion of adsorbed sulfate on the surface of the catalyst [1,28]. The bands at 986 and 1213 cm⁻¹ are the shift of 975 and 1208 cm⁻¹, due to their disappearance above 150 °C. However, the band at 1276 cm⁻¹ turns up at 200 °C, which can be assigned to the follow-up shift of 1213 cm⁻¹ [25,29,30]. At the same time, the band at 1363 cm⁻¹ may stem from asymmetric vibration of S–O bands of ammonium sulfate ((NH₄)₂SO₄) and grows in intensity over temperature [9,29]. The results indicate that there is no competitive adsorption between SO₂ and NO, and the adsorption of NH₃ on the catalyst can be promoted by adsorbed sulfate. Nevertheless, though SO₂ is surely adsorbed on the catalyst and sulfates are formed, the catalytic still maintains high activity, which is the same as before. It can be proposed that SO₂ is only adsorbed on specific sites on the catalyst and Ce⁴⁺ may be one of the specific sites according to a previous report [18].

2.6. H₂-TPR Analyses

To investigate the redox performance of the catalysts, H₂-TPR and H₂-TPR peak-differentiation-imitating of Mn-Ce-V-WO_x/TiO₂ catalyst profiles have been obtained, as Figure 6 shows. Figure 6A are the H₂-TPR curves of the catalysts. V₂O₅/TiO₂ shows a strong reduction peak at 428 °C, corresponding to the vanadia species reduction of V⁵⁺ → V³⁺ [31]. WO₃/TiO₂ shows two reduction peaks at 521 °C and 690 °C, and both of them are assigned to the reduction of W⁶⁺ → W⁴⁺ [32]. MnO₂/TiO₂ displays a wide reduction peak at 367 °C ascribed to the reduction of MnO₂ to Mn₂O₃ and Mn₂O₃ to Mn₃O₄ and a sharp reduction peak at 504 °C corresponds to the reduction of Mn₃O₄ to MnO [32–34]. The weak reduction peak for CeO₂/TiO₂ at 520 °C is caused by the reduction of low amount surface Ce⁴⁺ → Ce³⁺ [7,32,35]. Though the reference catalysts show multiple peaks in the temperature range of 300 °C to 800 °C, only one wide peak appears in the H₂-TPR profile of the catalyst with the molar ratio of 0.2 at 521 °C and peak shape is very wide,

which is due to the overlapping of multiple peaks, even the possible interaction among oxides on the support surface.

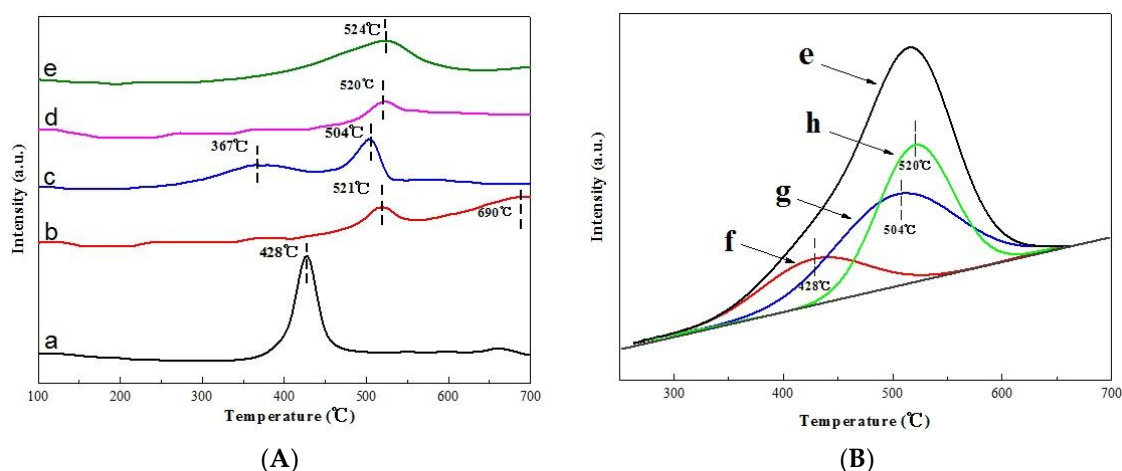


Figure 6. (A) H₂-Temperature programmed reduction (H₂-TPR) profiles of the catalysts: (a) V₂O₅/TiO₂; (b) WO₃/TiO₂; (c) MnO₂/TiO₂; (d) CeO₂/TiO₂; (e) Mn-Ce-V-WO_x/TiO₂ catalyst with molar ratio of 0.2. (B) H₂-TPR peak-differentiation-imitating of Mn-Ce-V-WO_x/TiO₂ catalyst: (e) Mn-Ce-V-WO_x/TiO₂ catalyst with molar ratio of 0.2; (f) the oxides of V; (g) the oxides of Mn; (h) the oxides of W and Ce.

To further investigate the important role of active components in the redox performance and the interaction among them, we have presented the H₂-TPR peak-differentiation-imitating of Mn-Ce-V-WO_x/TiO₂ catalyst in Figure 6B. Hydrogen consumption of single component catalysts and corresponding percent in composite catalysts have been listed in Table 1. Considering that the peak temperature of the WO₃ and CeO₂ is very close, peaks of the two oxides are unified into one peak here. The reduction peaks of one-component catalysts of V₂O₅ and MnO₂ are larger than those of WO₃ and CeO₂. However, in the composite catalyst, the single peak of MnO₂ and the overlap peak of CeO₂ and WO₃ are larger than the peak of V₂O₅, which is different from the redox properties of the four active components in the corresponding single-component catalysts. It can be inferred that the effect of Mn and Ce are more than superior water and sulfur resistance in the catalytic system. The interaction among the four active components enhances the redox properties of the oxides of the two elements. This can also be evidenced by the valence change of elements on the surface of the composite catalyst after H₂ reduction in the XPS below. It is well known that WO₃ acts as a promoter in traditional V₂O₅/WO₃-TiO₂ catalysts and contributes to the electron transfer among different valences of V element, which is also one of the main reasons for the high SCR activity of traditional catalysts; the oxide of Ce has a better ability to store and release oxygen. However, in the composite catalyst system, both the redox properties of Ce and W have been promoted, which shared part of the role of V₂O₅ with better redox ability in the catalytic activity. Therefore, both Ce and W contribute to the high NO conversion of the composite catalyst. The areas of reduction peaks of all oxides are different from the corresponding peaks of catalysts with a single component, which appeared in the case of the composite catalysts. The absolute amount of the four active components in the composite catalyst is less than that in the corresponding single-component catalysts, thus the hydrogen consumption of the four active components in the composite catalyst decreases. Among them, the reduction peaks of MnO₂ and CeO₂+WO₃ are strong but the reduction peak of V is relatively weak. The reduction of hydrogen consumption of V₂O₅ should not be attributed to the strong interaction among active components causing inhibition on V₂O₅ redox properties, but rather to the fact that in the composite catalyst, the amount of V₂O₅ is less than that in the other three active components. According to XPS test results, there is still a large amount of V₂O₅ that has been reduced in the composite catalyst. It can be inferred that they all play major roles in the redox reaction.

Table 1. Hydrogen consumption of single component catalysts and corresponding percent in composite catalyst.

	Catalysts							
	V2O5/TiO2	WO3/TiO2	MnO2/TiO2	CeO2/TiO2	Composite Catalyst	Peak of V ₂ O ₅	Peak of MnO ₂	Peak of WO ₃ + CeO ₂
Hydrogen consumption (μmol/g)	90.27	33.01	126.24	22.89	99.0	19.44	43.09	40.02

The results of H₂-TPR suggest that active components of the composite catalyst reveal characteristic redox properties, which is different from that of being alone, and the results indicate that the existence of a strong interaction among the active components on the surface of support is conducive to the promotion of reduction performance.

2.7. XPS Analysis

In the case of NO-SCR with NH₃ over the composite oxide catalyst, the catalyst will take part in the reaction, which has been reported extensively [13,36,37]. In order to obtain the information about the oxidation states of the active components on the catalyst, V 2p, W 4f, Mn 2p, Ce 3d and O 1s XPS spectra of the catalysts are recorded as shown in Figure 7. According to the literature, two main peaks are attributed to V 2p_{3/2} and V 2p_{1/2} in the V 2p XPS spectra [38,39]. However, in this work, only the V 2p_{3/2} level can be used to distinguish vanadium oxide species in different chemical states, and the peak of V 2p_{1/2} is very weak and hindered by O 1s satellites. The peaks of the catalysts are separated into three peaks at the binding energies of 515.6, 516.3 and 516.8 eV, assigned to V³⁺, V⁴⁺ and V⁵⁺, respectively [40–42]. Two main peaks in the W 4f XPS spectra are due to W 4f_{7/2} and W 4f_{5/2}, and the W 4f_{7/2} peak was divided into 34.6 (W⁵⁺) and 35.2 eV (W⁶⁺) and the W 4f_{5/2} peak is divided into 36.9 (W⁵⁺) and 37.7 eV (W⁶⁺), respectively [43,44]. Two main peaks assigned to Mn 2p_{3/2} and Mn 2p_{1/2} are observed, and the Mn 2p_{3/2} peaks are separated into three peaks at the binding energies of 640.3 ± 0.2, 641.3 ± 0.2 and 642.6 ± 0.2 eV, corresponding to Mn²⁺, Mn³⁺ and Mn⁴⁺, respectively [1,36,45]. The Ce 3d XPS spectra can be fitted into ten peaks: 880.3, 885.9, 898.8 and 903.9 eV assigned to Ce³⁺ and 882.5, 888.8, 898.4, 901.0, 907.5 and 916.7 eV associated with Ce⁴⁺. The O 1s peak is fitted into two sub-bands, one at 529.6 eV and the other at 531.1 eV, which can be attributed to the lattice oxygen O²⁻ and the surface adsorbed oxygen such as O₂²⁻, O⁻, O₂⁻ or OH⁻, respectively [13,46]. Compared with the XPS spectra of V 2p, W 4f and O 1s, Mn 2p and Ce 3d XPS spectra with the low intensity occur in 8 h using the composite catalyst with the molar ratio of 0.2 (shown in Figure 7C,D). The smaller nano-size and relative amount can lower the intensity of XPS spectra [45,47–49]. In this case, the low intensity can be attributed to sulfates covered on Mn and Ce species of the catalyst. Thus, the above conjecture that SO₂ adsorbed only on specific sites on the catalyst is proved to some extent.

The quantitative analyses of V, W, Mn, Ce and O species on the catalysts from XPS spectra have been listed in Table 2. For comparison, the quantitative analysis of each element after H₂ reduction has also been listed in Table 2. H₂ for the reduction of the catalyst is complete. The XPS analysis after reduction of H₂ shows that in the single-component catalysts, valence of V on the support surface is all converted from +5 to +3, and valence of Mn is also greatly converted from +4 to +2 and +3. Conversely, valence of W and Ce are relatively hard to be reduced, which proves the high redox properties of V and Mn compared to W and Ce as we know. However, the condition of valence change becomes different in the composite catalyst. It is easily determined that the proportion of different valence states of each element on a single active substance is quite different from those on the composite catalysts, which further indicates that the interaction exists among the oxides in the composite catalysts. The reduction of Mn increases, and the reduction of vanadium is only slightly reduced. It is worth noting that higher valence W and Ce are reduced, which is consistent with the result of H₂-TPR above. Interestingly, compared to the single-component catalysts, the amount of

oxygen adsorbed on the composite catalyst surface decrease. Through the TEM and HRTEM analysis, we know that the addition of four active components occupy more positions on the surface of support, resulting in an increase of acidic sites exposed on the surface, which can explain why the surface adsorption of oxygen decreases. Although there are references supporting that the increase of adsorbed oxygen can promote the SCR catalytic reaction, more importantly, the catalytic reaction involves a large number of electron transfer processes and it is clear that the diversity of valence states of the four active components and their high oxidation-reduction performance are the main reason for the high SCR performance in this system.

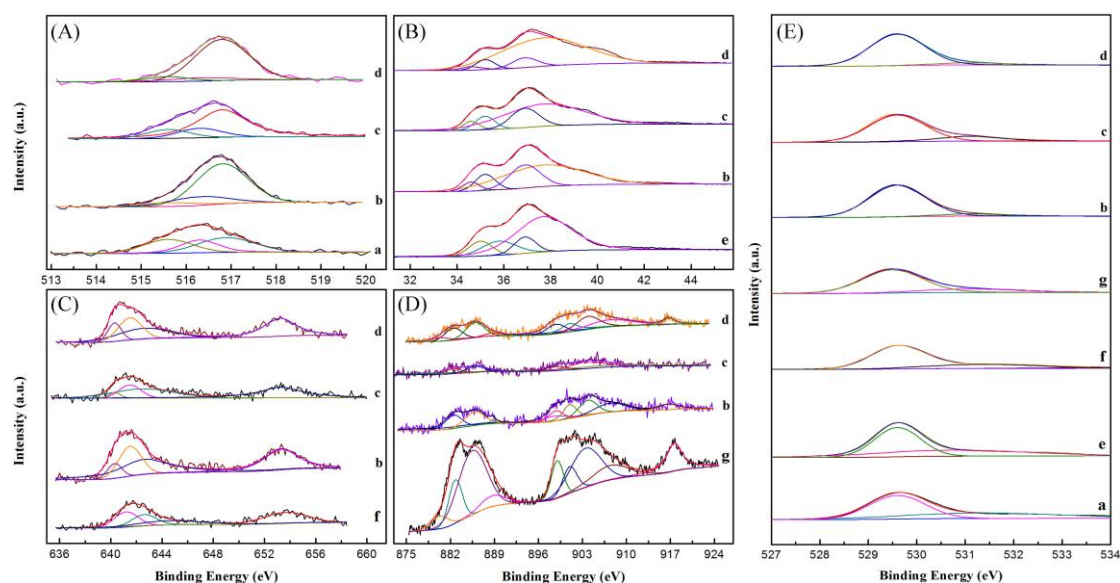


Figure 7. V 2p (A); W 4f (B); Mn 2p (C); Ce 3d (D) and O 1s (E) XPS spectra of the catalysts: (a) V_2O_5/TiO_2 ; (b) Fresh-catalyst with molar ratio of 0.2; (c) 8 h used-catalyst with molar ratio of 0.2; (d) 100 h used-catalyst with molar ratio of 0.2; (e) WO_3/TiO_2 ; (f) MnO_2/TiO_2 ; (g) CeO_2/TiO_2 .

Table 2. The percent of different valence states for V 2p, W 4f, Mn 2p, Ce 3d and O 1s.

Catalysts	Percent of Valence State, %											
	V 2p			W 4f		Mn 2p			Ce 3d		O 1s	
	V ³⁺	V ⁴⁺	V ⁵⁺	W ⁵⁺	W ⁶⁺	Mn ²⁺	Mn ³⁺	Mn ⁴⁺	Ce ³⁺	Ce ⁴⁺	Lattice Oxygen	Adsorbed Oxygen
V_2O_5/TiO_2	32.4	27.1	40.5	-	-	-	-	-	-	-	60.0	40.0
V_2O_5/TiO_2 **	100	0	0	-	-	-	-	-	-	-	53.5	46.5
WO_3/TiO_2	-	-	-	20.7	79.3	-	-	-	-	-	58.8	41.2
WO_3/TiO_2 **	-	-	-	46.8	53.2	-	-	-	-	-	58.4	41.6
MnO_2/TiO_2	-	-	-	-	-	3.9	52.7	43.5	-	-	68.7	31.3
MnO_2/TiO_2 **	-	-	-	-	-	22.3	61	16.7	-	-	28.1	71.9
CeO_2/TiO_2	-	-	-	-	-	-	-	-	40.3	59.7	80.4	19.6
CeO_2/TiO_2 **	-	-	-	-	-	-	-	-	46.1	53.9	63.5	36.5
Composite catalyst *	7.5	18.3	74.2	28.8	71.2	10.8	34.0	55.2	45.3	54.7	92.7	7.3
Composite catalyst **	79.9	3.6	16.5	54	46	35.4	50.2	14.4	60.6	39.4	78.9	21.1
Composite catalyst ***	14.1	15.9	70.0	24.2	75.8	6.9	30.8	62.3	57.3	42.7	80.2	19.8
Composite catalyst ****	7.9	9.0	83.1	10.8	89.2	18.3	38.5	43.2	47.3	52.7	92.5	7.5

* Fresh; ** After hydrogen reduction; *** 8 h used for resistance to H_2O and SO_2 ; **** 100 h used for stability test.

After the 100 h test, the concentration of O specie almost remains the same. Low valence state V and W species partly transform into the high valence state while high valence state Mn and Ce species partly convert into the low valence state. However, the change is faint, which corresponds with its superior stability. However, the concentrations of V, Mn, Ce and O species display a novel change compared with the fresh-catalyst after the 8 h H_2O and SO_2 resistance test. The concentration

of Ce^{4+} decreases, which can be caused by SO_2 . As a reducing agent, SO_2 induces a transformation from Ce^{4+} to Ce^{3+} on the surface, resulting in the formation of $\text{Ce}_2(\text{SO}_4)_3$ [20]. The decline of Mn^{2+} concentration may be owing to the sulfation on Mn^{2+} bound by SO_4^{2-} [50]. Furthermore, adsorption of H_2O and SO_2 on the sample can also affect the concentration of adsorbed oxygen, which makes it increase. Moreover, the increasing of V^{3+} concentration can be due to the enhanced adsorption of NH_3 by the sulfation on the catalyst surface. It can be inferred that the addition of manganese and cerium reduced the adverse effects of SO_2 on the catalytic activity owing to the result that SO_2 molecules are only adsorbed on Ce^{4+} and Mn^{2+} species on the composite catalyst.

3. Materials and Methods

3.1. Catalysts Preparation

All the catalysts were prepared by wet impregnation method. As active components, $\text{Mn}(\text{CH}_3\text{COO})_2$, NH_4VO_3 , $(\text{NH}_4)_{10}\text{W}_{12}\text{O}_{41}\cdot x\text{H}_2\text{O}$ (50 wt %) and $\text{Ce}(\text{NO}_3)_3\cdot 6\text{H}_2\text{O}$ with a molar ratio of 1:0.2:1:1 were completely dissolved in 60 mL citric acid solution (10 wt % $\text{C}_6\text{H}_8\text{O}_7\cdot\text{H}_2\text{O}$) and TiO_2 support powder was subsequently suspended in the obtained solution with the molar ratio of active components/ $\text{TiO}_2 = 0.1, 0.2, 0.3, 0.6$, respectively. The obtained mixture was stirred at room temperature for 1 h, then heated to 100 °C with stirring until the excess water was evaporated completely. The obtained solid was further dried at 120 °C for 12 h, and then calcined in air at 500 °C for 3 h. For comparison, $\text{V}_2\text{O}_5/\text{TiO}_2$, WO_3/TiO_2 , $\text{MnO}_2/\text{TiO}_2$, $\text{CeO}_2/\text{TiO}_2$, $\text{V}_2\text{O}_5\text{-WO}_3/\text{TiO}_2$, $\text{MnO}_2\text{-CeO}_2/\text{TiO}_2$, $\text{MnO}_2\text{-V}_2\text{O}_5\text{-WO}_3/\text{TiO}_2$ and $\text{CeO}_2\text{-V}_2\text{O}_5\text{-WO}_3/\text{TiO}_2$ catalysts with the same percentage content of corresponding active components were also prepared through the similar process.

3.2. NH_3 -SCR Activity Test

The SCR activity tests were carried out in a fixed-bed quartz reactor (0.3 mL catalyst; 40–60 mesh). The typical reactant gas composition contained: 1500 ppm NO, 1500 ppm NH_3 , 3% O_2 , 5 vol % H_2O (when added), 100 ppm SO_2 (when added) and balance Ar. The total gas flow rate was 200 mL/min and regulated by mass flow controllers (Sevenstar D08 series Flow Readout Boxed, Beijing Sevenstar Electronics Co., Ltd., Beijing, China), corresponding to the gas hourly space velocity (GHSV) of about 40,000 h^{-1} . The activity tests were examined at the temperature range of 100–400 °C. The NO outlet concentration was continuously monitored by the ThermoStar Gas Analysis System GSD320 analyzer (Pfeiffer Vacuum GmbH, Berlin, Germany).

3.3. Catalyst Characterization

XRD patterns were obtained using a D/MAX-3A Auto X-ray diffractometer (Rigaku Corporation, Tokyo, Japan) with $\text{Cu K}\alpha$ radiation. The X-ray source was operated at 40 kV and 40 mA. The diffraction patterns were taken in the 2θ range of 10–90° at a scan speed of 15° min^{-1} and a resolution of 0.02°. TEM and HRTEM were performed on a FEI Teccai G2S-Twin electron microscope (PHILIPS, Amsterdam, The Netherlands).

X-ray photoelectron spectra were obtained with K-Alpha spectrometer (Thermo Fisher Scientific, Waltham, MA, America) using $\text{Al K}\alpha$ (1486.7 eV) radiation as the excitation source with a precision of ± 0.3 eV. All binding energies were referenced to the C 1s line at 284.6 eV.

H_2 -TPR were performed on a sp-6801 gas chromatograph analyzer (Shandong Lunan Ruihong Chemical Instrument Co., Ltd., Tengzhou, China) using 0.1 g catalyst. The sample was first pretreated in Ar (30 mL \cdot min $^{-1}$) at 50 °C for 1 h and then heated up to 800 °C at a rate of 10 °C \cdot min $^{-1}$ under 5 vol % H_2/Ar . The consumption of H_2 was measured by a thermal conductivity detector (TCD, BEIJING BUILDER ELECTRONIC TECHNOLOGY CO., LTD., Beijing, China).

In situ FTIR spectra were recorded by a Fourier transform infrared spectrometer (Nicolet 6700, Thermo Fisher Scientific, Waltham, MA, America) equipped with a smart collector and MCT detector cooled by liquid N_2 , collecting 32 scans with a resolution of 4 cm^{-1} . The catalysts were firstly treated

at 500 °C in Ar for 1 h, then cooled down to 50 °C. Subsequently, the SCR reactant gas were introduced to the catalyst for 30 min, and then flushed with Ar for 10 min. The spectra were normally collected at temperatures ranging from 50 °C to 400 °C in a continuous NH₃ and NO flow. The background spectrum was recorded with the flowing of NH₃ and NO and subtracted from the sample spectrum.

4. Conclusions

Mn-Ce-V-WO_x/TiO₂ composite oxide catalysts with the molar ratio of active components/TiO₂ = 0.2, prepared by wet impregnation method, exhibit high NO conversion between 150 °C to 400 °C and good resistance to H₂O and SO₂ at 250 °C with a GHSV value of 40,000 h⁻¹. Four active components are well dispersed on TiO₂ surface and no crystalline phase is formed, but they can aggregate slightly, which is beneficial to the promotion of catalytic activity. NH₃ and NO are strongly adsorbed on the catalyst surface even at 400 °C, indicating that the catalyst still has a SCR reaction at this temperature. SO₂ is only adsorbed on Mn⁴⁺ and Ce⁴⁺ in this catalyst system, resulting in the formation of sulfates. However, the effect of Mn and Ce are more than superior water and sulfur resistance in the catalytic system. In addition, the characteristic redox properties of the catalyst are due to the existence of interaction among the active components on the support surface, and the interaction among them also enhances the redox properties of Ce and W oxides. Thus, all active components play major roles in the redox reaction, and the diversity of valence states of the four active components and their high oxidation-reduction performance are the main reason for the high SCR performance in this system.

Supplementary Materials: The following are available online at <http://www.mdpi.com/2073-4344/8/2/76/s1>, Figure S1: SCR activity test of two/three-component catalysts, Figure S2: XRD analysis of reference catalysts, Figure S3: HRTEM images of the composite oxide catalysts, Figure S4: The lifetime of Mn-Ce-V-WO_x/TiO₂ catalyst with 0.2 molar ratio.

Acknowledgments: The authors gratefully acknowledge financial support from the Fundamental Research Funds for the central universities (HEUCF20136910012), International Cooperation Special of The State Ministry of Science and Technology (2015DFR60380) and Advanced Technique Project Funds of The Manufacture and Information Ministry. And we thank Zhijuan Zhao and Xiaoyu Zhang from Analysis and Test Center of Chinese Sciences Academy Institute of Chemistry for their help in XPS.

Author Contributions: Guojun Dong conceived and designed the experiments; Xuteng Zhao performed the experiments; Lei Mao contributed reagents/materials/analysis tools; Xuteng Zhao and Lei Mao analyzed the data and wrote the paper.

Conflicts of Interest: The authors declare no conflict of interest.

References

1. Park, E.; Kim, M.; Jung, H.; Chin, S.; Jurng, J. Effect of Sulfur on Mn/Ti Catalysts Prepared Using Chemical Vapor Condensation (CVC) for Low-Temperature NO Reduction. *ACS Catal.* **2013**, *3*, 1518–1525. [CrossRef]
2. Boudali, L.K.; Ghorbel, A.; Grange, P. SCR of NO by NH₃ over V₂O₅ supported sulfated Ti-pillared clay: Reactivity and reducibility of catalysts. *Appl. Catal. A* **2006**, *305*, 7–14. [CrossRef]
3. Lónyi, F.; Solt, H.E.; Pászti, Z.; Valyon, J. Mechanism of NO-SCR by methane over Co,H-ZSM-5 and Co,H-mordenite catalysts. *Appl. Catal. B* **2014**, *150–151*, 218–229. [CrossRef]
4. Nicosia, D.; Czekaj, I.; Kröcher, O. Chemical deactivation of V₂O₅/WO₃-TiO₂ SCR catalysts by additives and impurities from fuels, lubrication oils and urea solution. *Appl. Catal. B* **2008**, *77*, 228–236. [CrossRef]
5. Si, Z.; Weng, D.; Wu, X.; Li, J.; Li, G. Structure, acidity and activity of CuOx/WOx-ZrO₂ catalyst for selective catalytic reduction of NO by NH₃. *J. Catal.* **2010**, *271*, 43–51. [CrossRef]
6. Thirupathi, B.; Smirniotis, P.G. Nickel-doped Mn/TiO₂ as an efficient catalyst for the low-temperature SCR of NO with NH₃: Catalytic evaluation and characterizations. *J. Catal.* **2012**, *288*, 74–83. [CrossRef]
7. Chen, L.; Li, J.; Ge, M. Promotional Effect of Ce-doped V₂O₅-WO₃/TiO₂ with Low Vanadium Loadings for Selective Catalytic Reduction of NOx by NH₃. *J. Phys. Chem. C* **2009**, *113*, 21177–21184. [CrossRef]

8. Xie, G.; Liu, Z.; Zhu, Z.; Liu, Q.; Ge, J.; Huang, Z. Simultaneous removal of SO₂ and NO_x from flue gas using a CuO/Al₂O₃ catalyst sorbentII. Promotion of SCR activity by SO₂ at high temperatures. *J. Catal.* **2014**, *224*, 42–49. [[CrossRef](#)]
9. Pan, S.; Luo, H.; Li, L.; Wei, Z.; Huang, B. H₂O and SO₂ deactivation mechanism of MnO_x/MWCNTs for low-temperature SCR of NO_x with NH₃. *J. Mol. Catal. A* **2013**, *377*, 154–161. [[CrossRef](#)]
10. Tian, Q.; Liu, H.; Yao, W.; Wang, Y.; Liu, Y.; Wu, Z.; Wang, H.; Weng, X. SO₂ Poisoning Behaviors of Ca-Mn/TiO₂ Catalysts for Selective Catalytic Reduction of NO with NH₃ at Low Temperature. *J. Nanomater.* **2014**, *2014*, 1–6. [[CrossRef](#)]
11. Xie, J.; Fang, D.; He, F.; Chen, J.; Fu, Z.; Chen, X. Performance and mechanism about MnO_x species included in MnO_x/TiO₂ catalysts for SCR at low temperature. *Catal. Commun.* **2012**, *28*, 77–81. [[CrossRef](#)]
12. Ettireddy, P.R.; Ettireddy, N.; Boningari, T.; Pardemann, R.; Smirniotis, P.G. Investigation of the selective catalytic reduction of nitric oxide with ammonia over Mn/TiO₂ catalysts through transient isotopic labeling and in situ FT-IR studies. *J. Catal.* **2012**, *292*, 53–63. [[CrossRef](#)]
13. Chen, Z.; Yang, Q.; Li, H.; Li, X.; Wang, L.; Tsang, S.C. Cr–MnO_x mixed-oxide catalysts for selective catalytic reduction of NO_x with NH₃ at low temperature. *J. Catal.* **2010**, *276*, 56–65. [[CrossRef](#)]
14. Zhang, D.; Zhang, L.; Shi, L.; Fang, C.; Li, H.; Gao, R.; Huang, L.; Zhang, J. In situ supported MnO(x)-CeO(x) on carbon nanotubes for the low-temperature selective catalytic reduction of NO with NH₃. *Nanoscale* **2013**, *5*, 1127–1136. [[CrossRef](#)] [[PubMed](#)]
15. Zhang, L.; Zhang, D.; Zhang, J.; Cai, S.; Fang, C.; Huang, L.; Li, H.; Gao, R.; Shi, L. Design of meso-TiO₂@MnO(x)-CeO(x)/CNTs with a core-shell structure as DeNO(x) catalysts: Promotion of activity, stability and SO₂-tolerance. *Nanoscale* **2013**, *5*, 9821–9829. [[CrossRef](#)] [[PubMed](#)]
16. Fang, C.; Zhang, D.; Cai, S.; Zhang, L.; Huang, L.; Li, H.; Maitarad, P.; Shi, L.; Gao, R.; Zhang, J. Low-temperature selective catalytic reduction of NO with NH₃ over nanoflaky MnO_x on carbon nanotubes in situ prepared via a chemical bath deposition route. *Nanoscale* **2013**, *5*, 9199–9207. [[CrossRef](#)] [[PubMed](#)]
17. Jin, R.; Liu, Y.; Wang, Y.; Cen, W.; Wu, Z.; Wang, H.; Weng, X. The role of cerium in the improved SO₂ tolerance for NO reduction with NH₃ over Mn-Ce/TiO₂ catalyst at low temperature. *Appl. Catal. B* **2014**, *148–149*, 582–588. [[CrossRef](#)]
18. Yang, S.; Guo, Y.; Chang, H.; Ma, L.; Peng, Y.; Qu, Z.; Yan, N.; Wang, C.; Li, J. Novel effect of SO₂ on the SCR reaction over CeO₂: Mechanism and significance. *Appl. Catal. B* **2013**, *136–137*, 19–28. [[CrossRef](#)]
19. Zhang, D.; Zhang, L.; Fang, C.; Gao, R.; Qian, Y.; Shi, L.; Zhang, J. MnO_x-CeO_x/CNTs pyridine-thermally prepared via a novel in situ deposition strategy for selective catalytic reduction of NO with NH₃. *RSC Adv.* **2013**, *3*, 8811–8819. [[CrossRef](#)]
20. Shu, Y.; Aikebaier, T.; Quan, X.; Chen, S.; Yu, H. Selective catalytic reaction of NO_x with NH₃ over Ce-Fe/TiO₂-loaded wire-mesh honeycomb: Resistance to SO₂ poisoning. *Appl. Catal. B* **2014**, *150–151*, 630–635. [[CrossRef](#)]
21. Thirupathi, B.; Smirniotis, P.G. Co-doping a metal (Cr, Fe, Co, Ni, Cu, Zn, Ce, and Zr) on Mn/TiO₂ catalyst and its effect on the selective reduction of NO with NH₃ at low-temperatures. *Appl. Catal. B* **2011**, *110*, 195–206. [[CrossRef](#)]
22. Tang, F.; Zhuang, K.; Yang, F.; Yang, L.; Xu, B.; Qiu, J.; Fan, Y. Effect of Dispersion State and Surface Properties of Supported Vanadia on the Activity of V₂O₅/TiO₂, Catalysts for the Selective Catalytic Reduction of NO by NH₃. *Chin. J. Catal.* **2012**, *33*, 933–940. [[CrossRef](#)]
23. Li, H.; Zhang, S.; Zhong, Q. Effect of nitrogen doping on oxygen vacancies of titanium dioxide supported vanadium pentoxide for ammonia-SCR reaction at low temperature. *J. Colloid Interface Sci.* **2013**, *402*, 190–195. [[CrossRef](#)] [[PubMed](#)]
24. Wu, Z.; Jiang, B.; Liu, Y.; Wang, H.; Jin, R. DRIFT Study of Manganese/Titania-Based Catalysts for Low-Temperature Selective Catalytic Reduction of NO with NH₃. *Environ. Sci. Technol.* **2007**, *41*, 5812–5817. [[CrossRef](#)] [[PubMed](#)]
25. Larrubia, M.A.; Ramis, G.; Busca, G. An FT-IR study of the adsorption of urea and ammonia over V₂O₅-MoO₃-TiO₂ SCR catalysts. *Appl. Catal. B* **2000**, *27*, L145–L151. [[CrossRef](#)]
26. Chen, L.; Li, J.; Ge, M. DRIFT Study on Cerium-Tungsten/Titania Catalyst for Selective Catalytic Reduction of NO_x with NH₃. *Environ. Sci. Technol.* **2010**, *44*, 9590–9596. [[CrossRef](#)] [[PubMed](#)]

27. Mihaylov, M.; Chakarova, K.; Hadjiivanov, K. Formation of carbonyl and nitrosyl complexes on titania-and zirconia-supported nickel: FTIR spectroscopy study. *J. Catal.* **2004**, *228*, 273–281. [[CrossRef](#)]
28. Zhao, L.; Li, X.; Hao, C.; Raston, C.L. SO₂ adsorption and transformation on calcined NiAl hydrotalcite-like compounds surfaces: An in situ FTIR and DFT study. *Appl. Catal. B* **2012**, *117–118*, 339–345. [[CrossRef](#)]
29. Liu, F.; Asakura, K.; He, H.; Shan, W.; Shi, X.; Zhang, C. Influence of sulfation on iron titanate catalyst for the selective catalytic reduction of NO_x with NH₃. *Appl. Catal. B* **2011**, *103*, 369–377. [[CrossRef](#)]
30. Vargas, M.A.L.; Casanova, M.; Trovarelli, A.; Busca, G. An IR study of thermally stable V₂O₅-WO₃-TiO₂ SCR catalysts modified with silica and rare-earths (Ce, Tb, Er). *Appl. Catal. B* **2007**, *75*, 303–311. [[CrossRef](#)]
31. Yu, W.; Wu, X.; Si, Z.; Weng, D. Influences of impregnation procedure on the SCR activity and alkali resistance of V₂O₅-WO₃/TiO₂ catalyst. *Appl. Surf. Sci.* **2013**, *283*, 209–214. [[CrossRef](#)]
32. Chang, H.; Li, J.; Yuan, J.; Chen, L.; Dai, Y.; Arandiyani, H.; Xu, J.; Hao, J. Ge, Mn-doped CeO₂-WO₃ catalysts for NH₃-SCR of NO_x: Effects of SO₂ and H₂ regeneration. *Catal. Today* **2013**, *201*, 139–144. [[CrossRef](#)]
33. Li, Q.; Yang, H.; Nie, A.; Fan, X.; Zhang, X. Catalytic Reduction of NO with NH₃ over V₂O₅-MnO_x/TiO₂-Carbon Nanotube Composites. *Catal. Lett.* **2011**, *141*, 1237–1242. [[CrossRef](#)]
34. Wang, Z.; Li, X.; Song, W.; Chen, J.; Li, T.; Feng, Z. Synergetic Promotional Effects Between Cerium Oxides and Manganese Oxides for NH₃-Selective Catalyst Reduction Over Ce-Mn/TiO₂. *Mater. Express* **2011**, *1*, 167–175. [[CrossRef](#)]
35. Cen, W.; Liu, Y.; Wu, Z.; Wang, H.; Weng, X. A theoretic insight into the catalytic activity promotion of CeO₂ surfaces by Mn doping. *Phys. Chem. Chem. Phys.* **2012**, *14*, 5769–5777. [[CrossRef](#)] [[PubMed](#)]
36. Wan, Y.; Zhao, W.; Tang, Y.; Li, L.; Wang, H.; Cui, Y.; Gu, J.; Li, Y.; Shi, J. Ni-Mn bi-metal oxide catalysts for the low temperature SCR removal of NO with NH₃. *Appl. Catal. B* **2014**, *148–149*, 114–122. [[CrossRef](#)]
37. Yang, S.; Wang, C.; Chen, J.; Peng, Y.; Ma, L.; Chang, H.; Chen, L.; Liu, C.; Xu, J.; Li, J.; et al. A novel magnetic Fe-Ti-V spinel catalyst for the selective catalytic reduction of NO with NH₃ in a broad temperature range. *Catal. Sci. Technol.* **2012**, *2*, 915–917. [[CrossRef](#)]
38. Gao, R.; Zhang, D.; Liu, X.; Shi, L.; Maitarad, P.; Li, H.; Zhang, J.; Cao, W. Enhanced catalytic performance of V₂O₅-WO₃/Fe₂O₃/TiO₂ microspheres for selective catalytic reduction of NO by NH₃. *Catal. Sci. Technol.* **2013**, *3*, 191–199. [[CrossRef](#)]
39. Nefzi, H.; Sediri, F. Vanadium oxide nanotubes VO_x-NTs: Hydrothermal synthesis, characterization, electrical study and dielectric properties. *J. Solid State Chem.* **2013**, *201*, 237–243. [[CrossRef](#)]
40. Guo, X.; Bartholomew, C.; Hecker, W.; Baxter, L.L. Effects of sulfate species on V₂O₅/TiO₂ SCR catalysts in coal and biomass-fired systems. *Appl. Catal. B* **2009**, *92*, 30–40. [[CrossRef](#)]
41. Boningari, T.; Koirala, R.; Smirniotis, P.G. Low-temperature catalytic reduction of NO by NH₃ over vanadia-based nanoparticles prepared by flame-assisted spray pyrolysis: Influence of various supports. *Appl. Catal. B* **2013**, *140–141*, 289–298. [[CrossRef](#)]
42. Yang, S.; Wang, C.; Ma, L.; Peng, Y.; Qu, Z.; Yan, N.; Chen, J.; Chang, H.; Li, J. Substitution of WO₃ in V₂O₅/WO₃-TiO₂ by Fe₂O₃ for selective catalytic reduction of NO with NH₃. *Catal. Sci. Technol.* **2013**, *3*, 161–168. [[CrossRef](#)]
43. Digregorio, F. Activation and isomerization of hydrocarbons over WO₃/ZrO₂ catalysts: I. Preparation, characterization, and X-ray photoelectron spectroscopy studies. *J. Catal.* **2004**, *225*, 45–55. [[CrossRef](#)]
44. Nishiguchi, T.; Oka, K.; Matsumoto, T.; Kanai, H.; Utani, K.; Imamura, S. Durability of WO₃/ZrO₂-CuO/CeO₂ catalysts for steam reforming of dimethyl ether. *Appl. Catal. A* **2006**, *301*, 66–74. [[CrossRef](#)]
45. Wang, L.; Huang, B.; Su, Y.; Zhou, G.; Wang, K.; Luo, H.; Ye, D. Manganese oxides supported on multi-walled carbon nanotubes for selective catalytic reduction of NO with NH₃: Catalytic activity and characterization. *Chem. Eng. J.* **2012**, *192*, 232–241. [[CrossRef](#)]
46. Shan, W.; Liu, F.; He, H.; Shi, X.; Zhang, C. A superior Ce-W-Ti mixed oxide catalyst for the selective catalytic reduction of NO_x with NH₃. *Appl. Catal. B* **2012**, *115–116*, 100–106. [[CrossRef](#)]
47. Gao, X.; Jiang, Y.; Zhong, Y.; Luo, Z.; Cen, K. The activity and characterization of CeO₂-TiO₂ catalysts prepared by the sol-gel method for selective catalytic reduction of NO with NH₃. *J. Hazard. Mater.* **2010**, *174*, 734–739. [[CrossRef](#)] [[PubMed](#)]

48. Wang, X.; Shi, A.; Duan, Y.; Wang, J.; Shen, M. Catalytic performance and hydrothermal durability of CeO₂-V₂O₅-ZrO₂/WO₃-TiO₂ based NH₃-SCR catalysts. *Catal. Sci. Technol.* **2012**, *2*, 1386–1395. [[CrossRef](#)]
49. Li, Q.; Hou, X.; Yang, H.; Ma, Z.; Zheng, J.; Liu, F.; Zhang, X.; Yuan, Z. Promotional effect of CeO_x for NO reduction over V₂O₅/TiO₂-carbon nanotube composites. *J. Mol. Catal. A* **2012**, *356*, 121–127. [[CrossRef](#)]
50. Yang, S.; Qi, F.; Liao, Y.; Xiong, S.; Lan, Y.; Fu, Y.; Shan, W.; Li, J. Dual Effect of Sulfation on the Selective Catalytic Reduction of NO with NH₃ over MnO_x/TiO₂: Key Factor of NH₃ Distribution. *Ind. Eng. Chem. Res.* **2014**, *53*, 5810–5819. [[CrossRef](#)]



© 2018 by the authors. Licensee MDPI, Basel, Switzerland. This article is an open access article distributed under the terms and conditions of the Creative Commons Attribution (CC BY) license (<http://creativecommons.org/licenses/by/4.0/>).